

THE EFFECT OF ROTATION PERIOD ON THERMAL STRESS WEATHERING. B. Ravaji^{1,2}, V. Ali-Lagoa³, M. Delbo⁴, J. Wilkerson^{1,5}, ¹Department of Mechanical Engineering, Texas A&M University, College Station, TX, USA (wilkerson@tamu.edu), ²Department of Mechanical Engineering, University of Texas at San Antonio, TX, USA, ³Max-Planck-Institut für extraterrestrische Physik, Giessenbachstasse, 1, 85748 Garching, Germany, ⁴UNS-CNRS, Observatoire de la Cote d'Azur, Boulevard de l'Observatoire-CS 34229, 06304 Nice Cedex 4, France, ⁵Department of Aerospace Engineering & Engineering Mechanics, University of Texas, Austin, TX, USA

Introduction: In most terrestrial environments, geomorphology is governed by a combination of physical, chemical, and biological processes with aeolian, fluvial, frost, and chemical processes being the primary drivers. In arid terrestrial environments many of these processes are inactive, and even fewer are active in airless, extraterrestrial environments [1,2].

Thermal stress weathering is now suspected to play an important role in rock breakdown, regolith generation, crater degradation, and landscape evolution in Earth's deserts and cold regions, Mars, Mercury, Moon, near-Earth asteroids, and perhaps comets [3,4,5]. Large diurnal temperature variations ($\Delta T > 100K$) and rapid rates-of-temperature-change ($dT/dt > 1 K/min$) are believed to be two key factors influencing the effectiveness of thermal stress weathering [3,4]. These two factors are greatly affected by orbital distance from Sun and rotation period. While the effect of orbital distance is fairly straightforward, i.e. thermal stress weathering is most effective at low perihelion, the effect of rotational period is non-trivial. In the current work, we study the role of rotation period on diurnal temperature variations and rates-of-temperature-change, and subsequently its role on thermal stresses and thermal stress weathering lifetime.

Physical process: For the present investigation, we make use of the thermal stress weathering model outlined in [3]. The model considers an unconstrained spherical rock on the surface of an asteroid, comet, moon, or airless planet that has a rotational period of P . As the rock rotates in relation to the Sun, it experiences oscillating temperature fields, governed by the heat equation, i.e. $dT/dt = \kappa \nabla^2 T$. Thermal stresses may arise due to both macroscopic spatial gradients in the temperature field and microscopic variations in thermal expansion due to material heterogeneities, e.g. chondrules in asteroids. Here, we refer to the former as macroscopic thermal stress and the latter as microscopic thermal stress. The combination of these macroscopic and microscopic thermal stresses, if of sufficient magnitude, can gradually drive progressive crack growth. Here, the thermal stress weathering lifetime of a rock is taken to be the time required for a thermal stress-driven crack to grow to sufficient size to fragment the rock. All necessary material properties

and model parameters are taken from [3] for the case of ordinary chondrites and S-type asteroids.

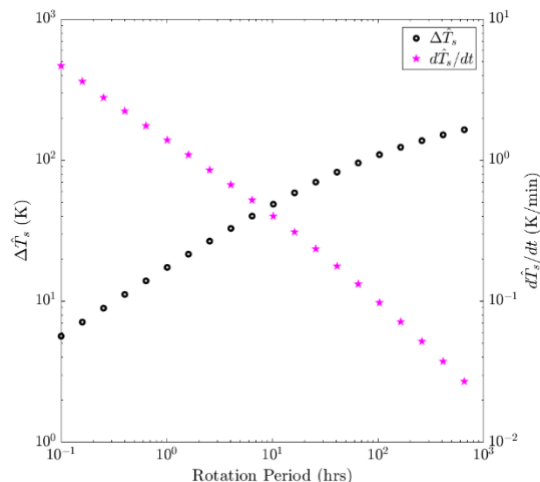


Fig. 1: Maximum diurnal surface temperature variation ($\Delta\hat{T}_s$) and maximum rate-of-surface-temperature-change ($d\hat{T}_s/dt$) of an S-type asteroid at 1 AU as a function of the asteroid's rotation period.

Model predictions: Fig. 1 presents model predictions (as black open circles) of the maximum diurnal surface temperature variation ($\Delta\hat{T}_s$) as a function of rotation period (P) for a rock on the surface of an S-type asteroid with an orbital distance of 1 AU. The maximum diurnal surface temperature variation increases monotonically with rotation period, i.e. larger on slow rotators. This result is to be expected, as slow rotators experience longer days and longer nights, thereby giving them more time to heat during the day and to cool during the night. On the other hand, fast rotators experience far less temperature variation, and in the limit of an infinitely fast rotator will experience zero temperature variation. These results would seem to suggest that thermal stress weathering is anticipated to be more effective on slow rotators, e.g. Moon ($P \sim 700$ hrs). That said, Fig. 1 also presents model predictions (as pink stars) of the maximum rate-of-temperature-change ($d\hat{T}_s/dt$) as a function of rotation period on the surface of an S-type asteroid with an orbital distance of 1 AU. The maximum rate-of-temperature-change increases with decreasing rotation

period, i.e. higher on fast rotators. Interestingly, this trend for $d\hat{T}_s/dt$ is opposite to that observed for $\Delta\hat{T}_s$, suggesting that thermal stress weathering could, perhaps, be effective on both slow and fast rotators, but for different underlying reasons.

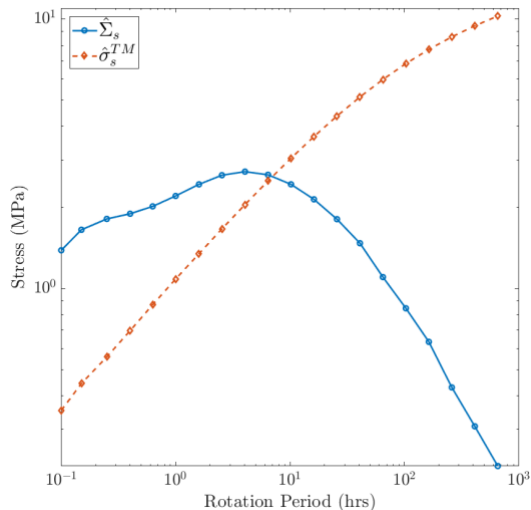


Fig. 2: Maximum microscopic ($\hat{\sigma}_s^{TM}$) and macroscopic ($\hat{\Sigma}_s$) surface stresses experienced by a rock with a diameter of 10 cm on the surface of an S-type asteroid at 1 AU as a function of the asteroid's rotation period.

Fig. 2 presents model predictions (open red diamonds) of the maximum microscopic stress at the surface, i.e. $\hat{\sigma}_s^{TM}$, of a rock with a diameter of 10 cm on the surface of an S-type asteroid at 1 AU as a function of rotation period. Interestingly, the trend for microscopic stress is nearly identical to that of $\Delta\hat{T}_s$ as shown in Fig. 1, i.e. monotonically increasing for slower rotation periods. This is to be expected, since microscopic stresses are linearly proportional to the local diurnal stresses are linearly proportional to the local diurnal temperature variation [3]. On the other hand, macroscopic stresses are far more complex, due to the fact that macroscopic stresses depend on the spatial distribution of the entire temperature field [4]. Fig. 2 provides model predictions (open blue circles) of the maximum surface macroscopic stress, i.e. $\hat{\Sigma}_s$, of the same rock as a function of rotation period. Here, the trend is non-monotonic, with $\hat{\Sigma}_s$ being highest for rotators with intermediate periods (i.e. $P \sim 6$ hrs) and lowest for slow rotators, e.g. Moon ($P \sim 700$ hrs). If $\hat{\Sigma}_s$ is a dominant factor in thermal stress weathering, then thermal stress weathering may be anticipated to be most effective on intermediate rotators. On the other hand, if microscopic thermal stress dominates, then thermal stress weathering may be more effective on slow rotators.

Finally, Fig. 3 reports model predictions (open black circles) of the thermal stress weathering lifetime of a 10-cm rock on the surface of an S-type asteroid at 1 AU as a function of the body's rotation period. Here, slow rotators, e.g. Moon, are predicted to have the longest thermal stress weathering lifetimes ($\sim 10^6$ - 10^7 years). Fast rotators generally have shorter thermal stress lifetimes, but the trend is somewhat non-monotonic. The slight non-monotonic effect is largely associated with the non-monotonic trend observed in the macroscopic stress, i.e. $\hat{\Sigma}_s$, as shown in Fig. 2.

Remarks on scaling thermal stress lifetimes: In [3] the thermal stress weathering lifetime was reported to be $\sim 10^3$ years for a 10-cm rock on an S-type asteroid at 1 AU for $P \sim 6$ hrs. An overly-simplified scaling has been proposed by [6] to scale this predicted lifetime for S-type asteroids to approximate the expected thermal stress weathering lifetime on the Moon with $P \sim 700$ hrs. The scaling was assumed to be linear with respect to period, and hence the thermal stress lifetime of a rock on the Moon was approximated to be $700/6$ times longer than that of a similar rock on an asteroid, i.e. $\sim 10^5$ years. As can be seen in Fig. 3, such a scaling is far too simplistic and can under-estimate the effect of rotation period on thermal stress weathering lifetime by two orders of magnitude.

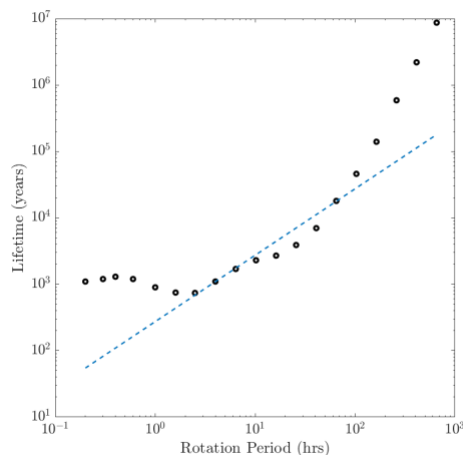


Fig. 3: Predicted thermal stress weathering lifetime of a rock of diameter 10 cm on the surface of an S-type asteroid at 1 AU as a function of the asteroid's rotation period. For comparison, a simple linear extrapolation is shown in the blue dashed curve.

References: [1] Hall K. (1999) *Geomorphology*, 31, 47–63. [2] Hallet. B. (2006) *Science*, 314, 1092-3. [3] Delbo M. et al. (2014) *Nature*, 508, 233–6. [4] Molaro J. et al. (2015) *JGRP*, 120, 255–77. [5] Alí-Lagoa, V. et al. (2015) *ApJL*, 810, L22. [6] Basilevsky A. et al. (2015), *PSS*, 117, 312-28.